Geophysical Research Letters

RESEARCH LETTER
10.1029/2021GL095051

How Are Under Ice Phytoplankton Related to Sea Ice in the Southern Ocean?

K. M. Bisson[1] and B. B. Cael[2]

[1]Oregon State University, Corvallis, OR, USA, [2]National Oceanography Centre, Southampton, UK

Key Points:

- Freeboard (ICESat-2) and under-ice plankton profiles (biogeochemical Argo floats) are compared via their probability distributions
- Freeboard variance, but not mean, is correlated to mean backscattering and chlorophyll maxima and the depths of these
- Freeboard may influence plankton via modulation of light penetration, mixed layer depth, and sea ice leads

Supporting Information:

Supporting Information may be found in the online version of this article.

Correspondence to:

K. M. Bisson,
bissonk@oregonstate.edu

Citation:

Bisson, K. M., & Cael, B. B. (2021). How are under ice phytoplankton related to sea ice in the Southern Ocean? *Geophysical Research Letters*, *48*, e2021GL095051. https://doi.org/10.1029/2021GL095051

Received 1 JUL 2021
Accepted 19 OCT 2021

Abstract Little is known about Southern Ocean under-ice phytoplankton, despite their suspected potential—ice and stratification conditions permitting—to produce blooms. We use a distributional approach to ask how Southern Ocean sea ice and under-ice phytoplankton characteristics are related, circumventing the dearth of co-located ice and phytoplankton data. We leverage all available Argo float profiles, together with freeboard (height of sea ice above sea level) and lead (ice fractures yielding open water) data from ICESat-2, to describe co-variations over time. We calculate moments of the probability distributions of maximum chlorophyll, particulate backscatter, the depths of these maxima, freeboard, and ice thickness. Argo moments correlate significantly with freeboard variance, lead fraction, and mixed layer depth, implying that sea ice dynamics drive plankton by modulating how much light they receive. We discuss ecological implications in the context of data limitations and advocate for diagnostic models and field studies to test additional processes influencing under-ice phytoplankton.

Plain Language Summary While sea ice undoubtedly influences under ice phytoplankton to some extent, little is known about under-ice phytoplankton in the Southern Ocean due to the paucity of field data. In the absence of plankton and ice measurements made at the same time and place, we can make inferences about the potential links between the two by comparing the average and variability of many measurements made within the same region. We do so with satellite-based measurements of freeboard (the thickness of sea ice above the water level) versus measurements made from profiling floats that measure plankton characteristics. We find that the average freeboard is unrelated to these plankton measures but that when freeboard is more variable, phytoplankton stocks tend to be higher and occur at shallower depths. These nonintuitive results encapsulate how plankton communities' response to light is complex, and suggest that plankton may respond positively to a more variable light field.

1. Introduction

Earth's polar regions are extreme ecosystems, marked by perennial darkness and seasonal mosaics of sea ice that modify the salinity, temperature, and incoming light of subsurface waters. Recent work in the Arctic has shown that phytoplankton can thrive underneath sea ice, dwarfing previous estimates for phytoplankton productivity across the annual cycle (Arrigo et al., 2012, 2014; Assmy et al., 2017), and raising questions of how sea ice influences under ice phytoplankton.

The effects of sea ice on phytoplankton in the Southern Ocean remains largely unknown as much research has focused on the Arctic Ocean, although more recent studies have expressed the possibility of widespread microbial life under Antarctic sea ice from observations (Arteaga et al., 2020; Cimoli et al., 2020; Hague & Vichi, 2021). Phytoplankton in the Southern Ocean are primarily limited by light and iron, and massive blooms under ice sea are generally not suspected in this region. However, nutrient replenishment from deeper Winter mixed layer depths combined with light at the onset of Spring may enable phytoplankton growth under ice. Still needed are assessments of how ice characteristics affect the under ice environment. On one hand, the thicker snow cover of Southern Ocean sea ice compared to the Arctic may prohibit the transmission of light to the waters below because the snow has a higher albedo than sea ice. On the other hand, most Antarctic sea ice melts in the Austral Spring and Summer (Pfirman et al., 1990), which may create a stable mixed layer and enhance growth of an already active under ice phytoplankton population previously living in deeper mixed layers (Hague & Vichi, 2021; Petty et al., 2014).

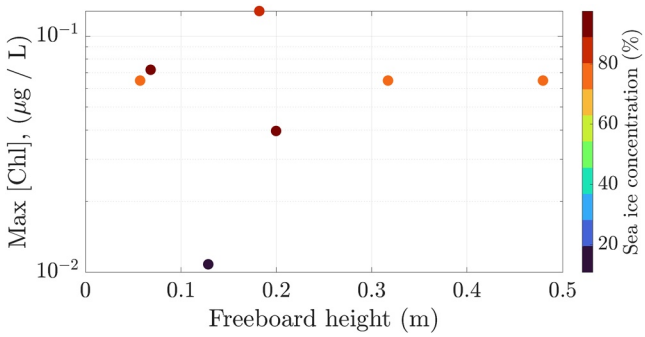

Figure 1. Maximum chlorophyll concentration of each under ice Argo profile is plotted against the same day freeboard from ICESat-2's ATL10 product, matched within a 25 km radius and colored by daily sea ice concentration values at a 25 × 25 km grid spacing. The Argo floats used in this plot are numbered "5,904,767," "5,905,995," and "5,905,102".

Antarctic sea ice extent has increased in recent decades (Holland, 2014; Maksym et al., 2012) (although this trend has reversed in recent years), and the Southern Ocean is predicted to experience enhanced precipitation (Emori & Brown, 2005; Vignon et al., 2021) in the coming years which will affect snow on sea ice processes (e.g., sea ice flooding as well as sea ice thinning via insulation Jacobs & Comiso, 1993), all of which will influence sea ice thickness and albedo to some extent (Arrigo et al., 2014; Maksym & Markus, 2008). Aside from physical processes, sea ice also directly influences the biogeochemistry of the water column (Tagliabue & Arrigo, 2006) and potential for phytoplankton growth, supplying up to 70% of the daily iron flux during melting periods (Lannuzel et al., 2007; Wang et al., 2014). As phytoplankton form the base of the marine ecosystem and as polar regions will continue to be modified by climate change, it is critical to document any relationships between phytoplankton and sea ice now, in order to both describe current conditions and to motivate future research directions.

Ideally, mechanistic relationships between sea ice and phytoplankton would be quantified using numerous coupled direct sea ice—phytoplankton observations from field campaigns spanning season and location to capture a spectrum in sea ice thickness, nutrient, and light limitations. Unfortunately, the scarcity of field measurements in the Southern Ocean severely limits any such investigation currently. Instead, remote observations from either underwater profiling floats (such as the Argo program Bittig et al., 2019; Roemmich et al., 2009) or lidar satellites (e.g., ICESat-2; Markus et al., 2017) greatly improve our ability to observe sea ice and water column properties during all times of the year. However, despite abundant remote observations from satellite and autonomous underwater floats, there are still very few same-day matchups of under ice phytoplankton and sea ice characteristics. As an illustration of this data paucity we plot the maximum chlorophyll concentration ([Chl], a pigment common to all phytoplankton) in the surface of an under ice float against the freeboard (height of sea ice above the sea surface), with ancillary information from daily sea ice concentration (Figure 1), totaling just seven observations of 1,020 total, or less than 1% of available observations. All points shown are within a radius of 25 km (a liberal range, given the phytoplankton decorrelation lengthscales in the Southern Ocean of 10–15 km Haëntjens et al., 2017; Bisson et al., 2020). Given that under ice [Chl], sea ice concentration, and freeboard are uncoupled in space and time, sea ice paired within 25 km of an under ice float profile may not share the same water mass, and variable sea ice features (i.e., deformation, ridges, leads) will adjust the under ice light environment in ways not explicitly accounted for this type of match-up comparison. Clearly, a paired-observation style analysis severely reduces the amount of available data and consequently reduces the questions that can be addressed regarding sea ice and phytoplankton.

While there are issues associated with using paired sea ice—phytoplankton data, it is plausible to expect some relationship between under ice biology and sea ice characteristics because sea ice influences light availability and mixed layer depths as mentioned above (see also Behrenfeld et al., 2017, Arteaga et al., 2020, and Behera et al., 2020). In this study, we employ a distributional approach to leverage all available under ice observations during the same time period as the ICESat-2 satellite. The advantage of a distributional approach is to relate the quantities of interest via their probability distributions' moments rather than on a point -per-point basis, and ultimately to learn how one underlying distribution may affect the other on broad scales of space and time. Distributional approaches have been used to identify new versus old ice apparent in the biomodal distributions of Arctic sea ice's total freeboard (e.g., Kwok et al., 2019), and these approaches have also been used to overcome data sparsity in linking ocean biological measurements across scales (Cael et al., 2018, 2021). Our aim here is to describe the variability of the under ice biological environment (via changes in the chlorophyll concentration and particulate backscattering, b_{bp}, which is known to covary with phytoplankton carbon) and to identify areas for future research.

2. Materials and Methods

2.1. Under Ice Argo Floats

Vertical under ice profiles of particulate backscattering (b_{bp}, m^{-1}, 700 nm hereafter referred to as b_{bp}) and adjusted chlorophyll concentration ([Chl], ug L^{-1}) were acquired from the Southern Ocean Carbon and Climate Observations and Modeling Project (SOCCOM). As in Bisson et al. (2019), profiles were despiked with a three point moving the median to remove contamination from bubbles and/or the presence of rare, large non-algal particles. Under ice, Argo profiles are flagged from an ice avoidant algorithm, which forces a float to retreat from its ascent if the median of the seven near surface (20–50 m depth) temperatures is less than −1.78 °C (Klatt et al., 2007). We removed profiles with sea ice concentration <15% (via satellite data, see Supporting Information S1) to be consistent with the ICESat-2 freeboard processing.

We also calculate mixed layer depth (MLD, see Supporting Information S1) for each float based on the density gradient method (Dong et al., 2008). The MLD is thought to exert a large control on phytoplankton growth based on both bottom-up processes (light and nutrients) as well as the concentration of phytoplankton exposed to grazing pressure (Arteaga et al., 2020; Behrenfeld et al., 2013). We also compare Argo characteristics with the mean temperature within the MLD, as the temperature is known to affect photosynthetic rates (Eppley, 1972). Altogether we note that the surface structure of under ice profiles is incomplete (due to missing surface data), and therefore our derived MLD is an imperfect approximation of the true MLD that may be achievable if the full profile were available. In total, we have 1,020 independent profiles across the shared time period of November 2018 to October 2020 where ATL20 data are available (more details in Supporting Information S1). Note, we do not include under ice Argo data from January to March, as sea ice extent is minimal during these times and there are only several Argo profiles available. Otherwise, the median number of Argo profiles available per given month and year is 51, with a range of 16–79 observations.

Rather than for example, calculating the median [Chl] and b_{bp} values within the mixed layer or euphotic depth (Bisson et al., 2019), we characterize under ice phytoplankton by reporting the maximum [Chl] and b_{bp} values within a profile as well as the depth at which a maximum is found. Deeper [Chl] maxima that do not co-occur with the maxima of b_{bp} may imply changes due to photoacclimation rather than enhanced biomass. In our data set, there are zero instances where the depth of maximum [Chl] or b_{bp} (hereafter z_c, z_b) is the shallowest depth in the profile, which suggests the reported z_c or z_b value is likely a good approximation of the true z_c or z_b value. One notable exception is if there are biomass peaks in the near surface (1–5 m) waters that are not captured with the floats, which can be the case for ice algae sloughing from the ice bottom from melting ice (Ardyna et al., 2020).

2.2. Sea Ice Data Products

We acquire total freeboard from ICESat-2 (Ice, Cloud, and land Elevation Satellite), distributed via the National Snow and Ice Data Center (NSIDC) and downloaded using Icepyx (Scheick, Arendt, Heagu, & Perez, 2019; Scheick, Arendt, Heagu, Paolo, et al., 2019). ICESat-2 was launched in October 2018 with the primary goal of quantifying cryosphere and terrestrial elevations with extremely high precision never before achieved from spacecraft (Markus et al., 2017). The primary instrument aboard ICESat-2 is Advanced Topographic Laser Altimeter System (ATLAS), which is a lidar that generates roughly 10,000 laser pulses per second and converts the time it takes for a small fraction of photons to return into a distance, and ultimately into a surface height. In this study, we use the ATL07, ATL10, and ATL20 products.

Sea ice types are provided in ATL07 (Kwok et al., 2021b) and are used to compute the fraction of sea ice segments that lead relative to the total segment length. While ICESat-2 delivers ungridded data in along-track granules, over the course of a month, the along-track segments approximate a 2D field (see Horvat et al., 2020). In this study, we use the specular lead (i.e., narrow gaps and fractures within the ice and between ice floes Petty et al., 2021), identification, which is determined from an empirical decision tree. ATL10 data (Kwok et al., 2021a) provide same-day freeboard for under ice Argo data shown in Figure 1. The ATL20 product (Petty et al., 2021) provides monthly means of freeboard (m) in 25 × 25 km pixels. Freeboard is determined from leads (which provide a reference sea surface height) along each beam from the ATL07 photon height product, and the data do not include cloudy conditions or when daily sea ice concentration

<15%. Only the strong beams were used in the analysis, and we use ICESat-2 products from October 2018 to October 2020.

Total freeboard (F, hereafter F from the ATL20 product) is the sum of sea ice and snow present above the ocean's surface. The total sea ice thickness (I, meters) will vary depending on the ratio of sea ice thickness to snow depth, or R. We calculate sea ice thickness in addition to F, where R values are calculated dynamically from F depending on the location of the sea ice (Li et al., 2018). We note that we choose to show our results using F rather than I due to the assumptions and error in calculating I, but choosing I rather than F did not change our results. Finally, daily gridded (25 × 25 km) sea ice concentration data were downloaded for the same day paired ATL10-Argo data shown in Figure 1. Argo and sea ice data were aggregated into unique year-month bins to facilitate comparison between both classes of data. We use these broad space/time constraints due to the location uncertainty in under ice floats as well as temporal resolution differences between Argo and ice data (which do not permit a point-by-point examination). We take Argo observations within a given month to be representative of that month, due to good spatial coverage of the Southern Ocean (See Supporting Information S1).

2.3. Statistical Framework

The complexity underlying the distributions of F, I, b_{bp}, [Chl], z_c, and z_b is distilled and described through the first three moments of each distribution: the mean, variance, and skewness. While the mean and variance describe the average and spread of the data, skewness quantifies how lopsided a distribution is relative to a perfectly symmetrical distribution (i.e., a positively skewed distribution has a heavier tail on the right side, meaning the mean exceeds the median). We calculate the mean, variance, and skewness for each distribution (i.e., b_{bp}, [Chl],z_b, z_c, F, I), for each unique month and year when data are available. Both b_{bp} and [Chl] are logarithmically distributed (i.e., span a large dynamic range) so we calculate their moments of the log-transformed variables. The strength of any relationships between variables is assessed through Kendall's τ, a non-parametric rank correlation.

We note that while b_{bp} and [Chl] both covary with phytoplankton biomass, neither variable perfectly quantifies phytoplankton. Although b_{bp} has better performance metrics with phytoplankton carbon compared to chlorophyll (see Graff et al., 2015), b_{bp} is imperfect as it also covaries with non-algal particles. For most of the year, the majority of particles under the ice will be phytoplankton, but there may be times in the Austral summer (e.g., export of fecal material and cell aggregates ; Moreau et al., 2020) when a portion of particles are non-algal. On the other hand, [Chl] is found in all phytoplankton, but it is plastic and varies with the light field. A change in [Chl] does not necessarily imply a change in biomass because cells can modify their pigment concentration according to irradiance levels. Both quantities are useful to assess phytoplankton under ice, and b_{bp} might be useful for assessing particles under the ice for times of the year when particles are expected.

3. Temporal Patterns in Under Ice Properties

Distributions of b_{bp} and [Chl] show clear seasonality for the month and year pairings when all data are available (Figure 2). The maximum F occurs in December and there are subtle shifts in the width of F throughout the annual cycle, with June and July representing the least variable F distributions in both 2019 and 2020.

The shapes of maximum b_{bp} vary tremendously from month to month across the annual cycle, with long tails of b_{bp} in October–December, and shorter tails in June and July. There are times of the year when the distribution of b_{bp} is unimodal, and other times when it's roughly bimodal (e.g., December 2018, May 2019, September–December 2019, August–September 2020). Like b_{bp}, [Chl] distributions tend to have longer tails from October - December, but unlike b_{bp}, [Chl] distributions tend to be left-skewed from April to June. In general [Chl] has wider distributions throughout the annual cycle compared to b_{bp}.

The seasonal cycle in b_{bp} and [Chl] is more pronounced than that of F or z_b and z_c. Previous work found that under ice phytoplankton growth initiates before melting (Hague & Vichi, 2021), and also that phytoplankton can grow under low light conditions compared to what was previously thought in the Antarctic

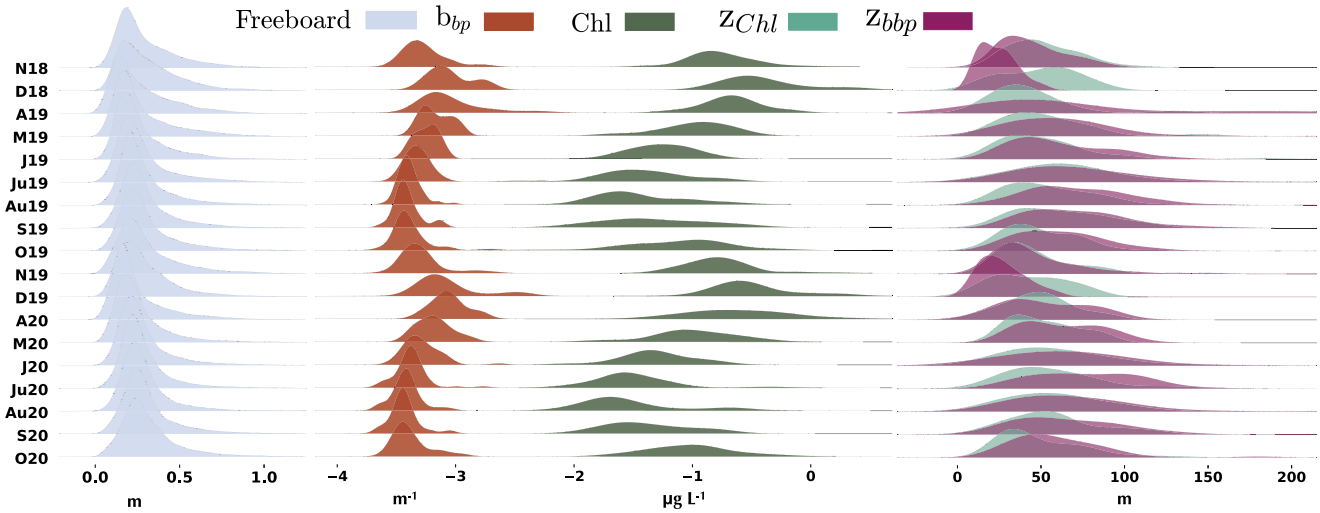

Figure 2. Ridge plot comparing probability density functions of F (gray, left), b_{bp} (orange, log10 transformed), [Chl] (green, log10 transformed), z_c (teal), and z_b (purple) across month (y-axis). Note that January–March are not shown and are not included in analyses because there are too few Argo observations in those months.

(Arteaga et al., 2020). Our work is in broad agreement with these studies, especially as there are long tails in the distribution of b_{bp} and [Chl] from August through September, implying more instances of anomalously high biomass.

What differences in the distributions of sea ice and phytoplankton characteristics might be expected? For example, b_{bp} or [Chl] reflect a balance between phytoplankton growth and losses, ultimately depending on the light and nutrient environment as well as viral activity and grazing pressure. Photoacclimation and physical mixing in the water column influence z_b and z_c, including algae released into waters from the base of melting sea ice (Yoshida et al., 2020). One might expect enhanced b_{bp} and [Chl] with decreasing $\mu(F)$ and $\mu(I)$ if phytoplankton are primarily light limited. If algae living in sea ice are a dominant control on variability in z_b or z_c, we expect z_b and z_c will shoal in tandem with melting ice.

There are seasonal patterns in the distributions of z_b and z_c as well, where the mean z_b is usually much less than z_c during November and December, but z_b slightly exceeds z_c during Winter and Spring. The former might imply a flux of algae and their aggregates into the water from melting sea ice (Moreau et al., 2020), and/or possibly fecal pellets from krill feeding on algal ice populations at the near surface (Arrigo & Thomas, 2004). We note that algal ice is expected to contribute a greater fraction of productivity (relative to the in water phytoplankton) in October and November (Lizotte, 2001), so it is plausible that there could be enhanced export flux (i.e., higher particle loads, or enhanced $\mu(b_{bp})$ relative to μ[Chl]) in November and December. A combination of sloughing algae from sea ice, as well as export of particles (including senescent algal cells), might create bimodal distributions in b_{bp}, [Chl], z_b and z_c, as is observed to different degrees from September through December.

4. Relating Distributions Through Their Moments

A distributional approach doesn't provide causal links between sea ice and phytoplankton, but it is nevertheless useful to identify what the current data suggests. The Argo moments (in particular the mean, $\mu(\cdot)$) correlate moderately well with ice variance ($\sigma(\cdot)$) and ice skewness but not with ice mean (Figure 3). Both $\mu(b_{bp})$ and μ([Chl]) increase with increasing ice variance, and $\mu(z_c)$ and $\mu(z_b)$ decrease with increasing $\sigma(F)$. In general, the Argo σ moments do not relate well to ice moments, with the exception of $\sigma(b_{bp})$, which is positively correlated with $\sigma(F)$. $\mu(z_b)$ increases with increasing ice skewness. Put another way, a variable ice environment coincides with higher b_{bp} and [Chl] at shallower depths. Months with greater proportions of thicker ice have deeper depths of maximum b_{bp}. Neither $\mu(b_{bp})$ nor μ[Chl] are significantly correlated with statistical moments of temperature (p values exceed 0.1 in all cases, and generally exceed 0.5).

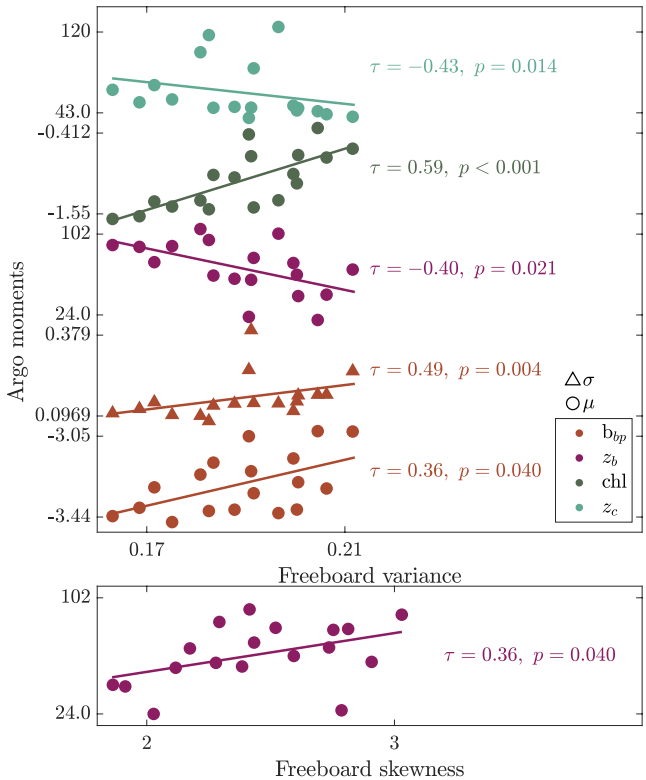

Figure 3. Trends in Argo moments and ice variance (top panel) as well as Argo z_b and ice skewness (bottom panel) across Argo variates (b_{bp}, [Chl], z_b and z_c). For top plot, separate y-ticks are given for each moment-variable combination to show their ranges. Note that b_{bp} and [Chl] are shown in log-scales, and all points are the monthly values.

MLD correlates most strongly and negatively with phytoplankton (μ(MLD) and $\mu(b_{bp})$ have a τ of −0.73 and a p-value < 0.005, while μ(MLD) and μ([Chl]) have a τ of −0.54 and a p-value < 0.005), evincing that light exerts a strong control over phytoplankton in this study. We cannot assess the role of nutrients (and iron in particular) in this study due to lack of data, and therefore cannot say, for example, if iron versus sea ice and MLD has a stronger influence on phytoplankton under ice.

The presence of significant, moderate correlations between sea ice variance and Argo moments, as opposed to the weak correlations between sea ice mean and Argo moments, implies that variance in ice thickness is more influential than mean ice thickness for phytoplankton growth. The negative relationship between ice variance and $\mu(z_b)$ is somewhat counter intuitive, as one might expect z_b to become more variable as ice variance increases.

However, if the relationship between F and plankton characteristics is nonlinear, it is plausible that $\sigma(F)$ is what drives greater and shallower plankton stocks. Light transmission through sea ice is $\propto e^{-k}$F (Beer's law) for a given k related to sea ice properties. As light penetration decreases nonlinearly with ice thickness, there's a greater difference in light transmission through F of for example, 0 and 1 m than between 1 and 2 m, and so on as F increases. All other factors constant, average light penetration in a region is affected by how much of the total ice is sufficiently thin to permit light transmission, and by how thick ice is in this area—in other words, the low tail of F. The low tail of F is best captured by $\sigma(F)$ given that F is positively skewed, so ultimately, this low tail of small-F values can be what dominates total light penetration, and hence plankton characteristics.

Underlying the statistically significant relationships of sea ice, MLD, and phytoplankton are possible mechanistic explanations. The near seasonality in b_{bp} and [Chl], coupled with the correlations of Argo moments to ice variance and leads implies leads and/or thin sea ice permit light to reach the phytoplankton at all times of the year to varying degrees (Figure 4). Indeed, the seasonal cycle of maximum b_{bp} tracks very well with the sea ice specular lead fraction (Figure 4, note that Spearman's rank correlation between lead fraction and $\mu(b_{bp})$ is 0.78, and $\tau = 0.58$), where higher specular lead fractions also coincide with greater incident photosynthetically active radiation in the Southern Ocean and more shallow MLD. Under ice phytoplankton are mobile, embedded in water masses transiting beneath both snow covered ice and brief exposure to open water, and consequently are likely to experience intermittent pulses of light that they may have adapted to use efficiently.

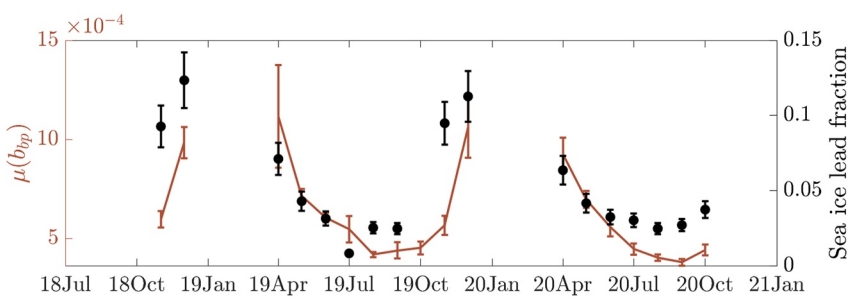

Figure 4. Time series of $\mu(b_{bp})$ (m^{-1}) using all available under ice Argo data and the sea ice lead fraction of specular leads (gaps and fractures between ice floes). Error bars represent the coefficient of variation for each month.

Our findings differ with those of the Lowry et al. (2018) study, which found that leads inhibited phytoplankton blooms via convective mixing in the Arctic Ocean. In the Southern Ocean, we found that a higher fraction of leads corresponds to larger maxima in under ice [Chl] that occur at more shallow depths, which is most similar to the findings of Assmy et al. (2017) in the Arctic Ocean. The magnitude of under ice [Chl] in the Southern Ocean is generally less than that of Arctic blooms, but the magnitude of under ice [Chl] in the Southern Ocean is comparable (at times exceeding) to that of the ice-free areas of the Southern Ocean (Haëntjens et al., 2017; Rembauville et al., 2017; i.e., in this study the maximum [Chl] is 8 μg per L).

5. Concluding Remarks

We have employed a statistical approach as a way to overcome the shortage of data. Although there are numerous measurements of either Argo of ICESat-2 observations by themselves, there were no true paired observations between ICESat-2 and Argo. The inherent position uncertainty associated with under ice Argo floats almost certainly means no exact match ups (i.e., those within reasonable space and time constraints) between Argo and any other sensor can be expected in the future unless under ice acoustic positioning can help decrease position uncertainty. Still, the continued presence of Argo floats in the Southern Ocean will undoubtedly help to address the role of sea ice and phytoplankton growth. Ideally, all SOCCOM Argo floats would be equipped with photosynthetically active radiation sensors, unlike those used herein. While there were sufficient profiles in this study to examine monthly distributions, we could not examine regional differences due to the data set size. In the coming years, more under ice data will become available and perhaps permit such an analysis. Here we found enhanced phytoplankton biomass and variability with decreasing MLD, increasing F variance, and increasing lead fractions, which might plausibly be explained by factors not addressed in this study (i.e., spatial differences in iron availability and grazing pressure).

Despite the limitations, statistical approaches remain useful to understand general patterns in under-ice phytoplankton, and time series analyses will become important as more data become available in the coming decades. In order to build a mechanistic understanding of phytoplankton under sea ice, synergistic models could incorporate data from Argo with other platforms. Large-scale climate modeling is also important for assessing the likelihood of phytoplankton growth based on environmental conditions (e.g., ice cover, MLD) that might be informed from our findings here.

Neither models nor statistical methods replace fieldwork. We recommend field studies incorporating under ice light, phytoplankton, and zooplankton in particular, as well as measuring sea-ice algal communities (Cimoli et al., 2017). Under the ice, phytoplankton blooms have commonly been treated as the result of bottom-up processes (i.e., light and nutrient status), and our study focused on ice and phytoplankton characteristics. More Information about nutrient status, zooplankton (perhaps from the deployment of imaging sensors, such as the Underwater Vision Profiler), and other heterotrophic activity would help to more explicitly characterize the many mechanisms influencing phytoplankton under sea ice beyond what has been considered here.

Acknowledgments
The authors are grateful to Ted Maksym, Emmanuel Boss, and Chris Horvat for helpful conversations, to the Icepyx team (especially Jessica Scheick, Romina Piunno, and Rachel Tilling), and to the ICESat-2 science team and project office for their support. We thank Sébastien Moreau and Emma Cavan for their help in improving our manuscript. Argo data were collected and made freely available by the Southern Ocean Carbon and Climate Observations and Modeling (SOCCOM) Project funded by the National Science Foundation, Division of Polar Programs (NSF PLR -1,425,989 and OPP-1936222), supplemented by NASA, and by the International Argo Program and the NOAA programs that contribute to it (https://soccompu.princeton.edu/www/index.html). K. M. Bisson acknowledges NASA Grant 80NSSC20K0970. B. B. Cael acknowledges support by the National Environmental Research Council Grant NE/T010622/1 CELOS (Constraining the EvoLution of the Southern Ocean carbon Sink).

Data Availability Statement

The Argo Program is part of the Global Ocean Observing System. ICEsat-2 data can be accessed via https://nsidc.org/data/atl07. The full Argo archive is available at https://doi.org/10.17882/42182.

References

Ardyna, M., Mundy, C., Mayot, N., Matthes, L. C., Oziel, L., Horvat, C., et al. (2020). Under-ice phytoplankton blooms: Shedding light on the "invisible" part of arctic primary production. *Frontiers in Marine Science*, *7*, 985. https://doi.org/10.3389/fmars.2020.608032

Arrigo, K. R., Perovich, D. K., Pickart, R. S., Brown, Z. W., Van Dijken, G. L., Lowry, K. E., et al. (2012). Massive phytoplankton blooms under Arctic sea ice. *Science*, *336*(6087), 1408. https://doi.org/10.1126/science.1215065

Arrigo, K. R., Perovich, D. K., Pickart, R. S., Brown, Z. W., van Dijken, G. L., Lowry, K. E., et al. (2014). Phytoplankton blooms beneath the sea ice in the Chukchi sea. *Deep Sea Research Part II: Topical Studies in Oceanography*, *105*, 1–16. https://doi.org/10.1016/j.dsr2.2014.03.018

Arrigo, K. R., & Thomas, D. N. (2004). Large scale importance of sea ice biology in the southern ocean. *Antarctic Science*, *16*(4), 471–486. https://doi.org/10.1017/s0954102004002263

Arteaga, L. A., Boss, E., Behrenfeld, M. J., Westberry, T. K., & Sarmiento, J. L. (2020). Seasonal modulation of phytoplankton biomass in the southern ocean. *Nature Communications*, *11*(1), 1–10. https://doi.org/10.1038/s41467-020-19157-2

Assmy, P., Fernández-Méndez, M., Duarte, P., Meyer, A., Randelhoff, A., Mundy, C. J., et al. (2017). Leads in Arctic pack ice enable early phytoplankton blooms below snow-covered sea ice. *Scientific Reports*, *7*(1), 1–9. https://doi.org/10.1038/srep40850

Behera, N., Swain, D., & Sil, S. (2020). Effect of Antarctic sea ice on chlorophyll concentration in the southern ocean. *Deep Sea Research Part II: Topical Studies in Oceanography*, *178*, 104853. https://doi.org/10.1016/j.dsr2.2020.104853

Behrenfeld, M. J., Doney, S. C., Lima, I., Boss, E. S., & Siegel, D. A. (2013). Annual cycles of ecological disturbance and recovery underlying the subarctic Atlantic spring plankton bloom. *Global Biogeochemical Cycles*, *27*(2), 526–540. https://doi.org/10.1002/gbc.20050

Behrenfeld, M. J., Hu, Y., O'Malley, R. T., Boss, E. S., Hostetler, C. A., Siegel, D. A., et al. (2017). Annual boom–bust cycles of polar phytoplankton biomass revealed by space-based lidar. *Nature Geoscience*, *10*(2), 118–122. https://doi.org/10.1038/ngeo2861

Bisson, K., Boss, E., Werdell, P., Ibrahim, A., & Behrenfeld, M. (2020). Particulate backscattering in the global ocean: A comparison of independent assessments. *Geophysical Research Letters*, *48*, e2020GL090909.

Bisson, K., Boss, E., Westberry, T., & Behrenfeld, M. (2019). Evaluating satellite estimates of particulate backscatter in the global open ocean using autonomous profiling floats. *Optics Express*, *27*(21), 30191–30203. https://doi.org/10.1364/oe.27.030191

Bittig, H. C., Maurer, T. L., Plant, J. N., Schmechtig, C., Wong, A. P., Claustre, H., et al. (2019). A bgc-argo guide: Planning, deployment, data handling and usage. *Frontiers in Marine Science*, *6*, 502. https://doi.org/10.3389/fmars.2019.00502

Cael, B., Bisson, K., Conte, M., Duret, M. T., Follett, C. L., Henson, S. A., et al. (2021). Open ocean particle flux variability from surface to seafloor. *Geophysical Research Letters*, *48*(9), e2021GL092895. https://doi.org/10.1029/2021gl092895

Cael, B., Bisson, K., & Follett, C. L. (2018). Can rates of ocean primary production and biological carbon export be related through their probability distributions? *Global Biogeochemical Cycles*, *32*(6), 954–970. https://doi.org/10.1029/2017gb005797

Cimoli, E., Lucieer, A., Meiners, K. M., Lund-Hansen, L. C., Kennedy, F., Martin, A., et al. (2017). Towards improved estimates of sea-ice algal biomass: Experimental assessment of hyperspectral imaging cameras for under-ice studies. *Annals of Glaciology*, *58*(75pt1), 68–77. https://doi.org/10.1017/aog.2017.6

Cimoli, E., Lucieer, V., Meiners, K. M., Chennu, A., Castrisios, K., Ryan, K. G., & Lucieer, A. (2020). Mapping the in situ microspatial distribution of ice algal biomass through hyperspectral imaging of sea-ice cores. *Scientific Reports*, *10*(1), 1–17. https://doi.org/10.1038/s41598-020-79084-6

Dong, S., Sprintall, J., Gille, S. T., & Talley, L. (2008). Southern ocean mixed-layer depth from argo float profiles. *Journal of Geophysical Research: Oceans*, *113*(C6). https://doi.org/10.1029/2006jc004051

Emori, S., & Brown, S. (2005). Dynamic and thermodynamic changes in mean and extreme precipitation under changed climate. *Geophysical Research Letters*, *32*(17). https://doi.org/10.1029/2005gl023272

Eppley, R. W. (1972). Temperature and phytoplankton growth in the sea. *Fishery Bulletin*, *70*(4), 1063–1085.

Graff, J. R., Westberry, T. K., Milligan, A. J., Brown, M. B., Dall'Olmo, G., van Dongen-Vogels, V., et al. (2015). Analytical phytoplankton carbon measurements spanning diverse ecosystems. *Deep Sea Research Part I: Oceanographic Research Papers*, *102*, 16–25. https://doi.org/10.1016/j.dsr.2015.04.006

Haëntjens, N., Boss, E., & Talley, L. D. (2017). Revisiting ocean color algorithms for chlorophyll a and particulate organic carbon in the southern ocean using biogeochemical floats. *Journal of Geophysical Research: Oceans*, *122*(8), 6583–6593. https://doi.org/10.1002/2017jc012844

Hague, M., & Vichi, M. (2021). Southern ocean biogeochemical Argo detect under-ice phytoplankton growth before sea ice retreat. *Biogeosciences*, *18*(1), 25–38. https://doi.org/10.5194/bg-18-25-2021

Holland, P. R. (2014). The seasonality of Antarctic sea ice trends. *Geophysical Research Letters*, *41*(12), 4230–4237. https://doi.org/10.1002/2014gl060172

Horvat, C., Blanchard-Wrigglesworth, E., & Petty, A. (2020). Observing waves in sea ice with ICESat-2. *Geophysical Research Letters*, *47*(10), e2020GL087629. https://doi.org/10.1029/2020gl087629

Jacobs, S. S., & Comiso, J. C. (1993). A recent sea-ice retreat west of the antarctic peninsula. *Geophysical Research Letters*, *20*(12), 1171–1174. https://doi.org/10.1029/93gl01200

Klatt, O., Boebel, O., & Fahrbach, E. (2007). A profiling float's sense of ice. *Journal of Atmospheric and Oceanic Technology*, *24*(7), 1301–1308. https://doi.org/10.1175/jtech2026.1

Kwok, R., Markus, T., Kurtz, N., Petty, A., Neumann, T., Farrell, S., et al. (2019). Surface height and sea ice freeboard of the arctic ocean from ICESat-2: Characteristics and early results. *Journal of Geophysical Research: Oceans*, *124*(10), 6942–6959. https://doi.org/10.1029/2019jc015486

Kwok, R., Petty, A., Cunningham, G., Markus, T., Hancock, D., Ivanoff, A., et al. (2021a). *Atlas/ICESat-2 l3a sea ice freeboard, version 4*. NSIDC: National Snow and Ice Data Center.

Kwok, R., Petty, A., Cunningham, G., Markus, T., Hancock, D., Ivanoff, A., et al. (2021b). *Atlas/ICESat-2 l3a sea ice height, version 4*. NSIDC: National Snow and Ice Data Center.

Lannuzel, D., Schoemann, V., De Jong, J., Tison, J.-L., & Chou, L. (2007). Distribution and biogeochemical behaviour of iron in the east Antarctic Sea Ice. *Marine Chemistry*, *106*(1–2), 18–32. https://doi.org/10.1016/j.marchem.2006.06.010

Li, H., Xie, H., Kern, S., Wan, W., Ozsoy, B., Ackley, S., & Hong, Y. (2018). Spatio-temporal variability of Antarctic Sea-Ice thickness and volume obtained from ICESat data using an innovative algorithm. *Remote Sensing of Environment*, *219*, 44–61. https://doi.org/10.1016/j.rse.2018.09.031

Lizotte, M. P. (2001). The contributions of sea ice algae to Antarctic marine primary production. *American Zoologist*, *41*(1), 57–73. https://doi.org/10.1093/icb/41.1.57

Lowry, K. E., Pickart, R. S., Selz, V., Mills, M. M., Pacini, A., Lewis, K. M., et al. (2018). Under-ice phytoplankton blooms inhibited by spring convective mixing in refreezing leads. *Journal of Geophysical Research: Oceans*, *123*(1), 90–109. https://doi.org/10.1002/2016jc012575

Maksym, T., & Markus, T. (2008). Antarctic sea ice thickness and snow-to-ice conversion from atmospheric reanalysis and passive microwave snow depth. *Journal of Geophysical Research: Oceans*, *113*(C2). https://doi.org/10.1029/2006jc004085

Maksym, T., Stammerjohn, S. E., Ackley, S., & Massom, R. (2012). Antarctic sea ice—A polar opposite? *Oceanography*, *25*(3), 140–151. https://doi.org/10.5670/oceanog.2012.88

Markus, T., Neumann, T., Martino, A., Abdalati, W., Brunt, K., Csatho, B., et al. (2017). The ice, cloud, and land elevation satellite-2 (ICESat-2): Science requirements, concept, and implementation. *Remote Sensing of Environment*, *190*, 260–273. https://doi.org/10.1016/j.rse.2016.12.029

Moreau, S., Boyd, P. W., & Strutton, P. G. (2020). Remote assessment of the fate of phytoplankton in the southern ocean sea-ice zone. *Nature Communications*, *11*(1), 1–9. https://doi.org/10.1038/s41467-020-16931-0

Petty, A., Bagnardi, M., Kurtz, N., Tilling, R., Fons, S., Armitage, T., & Kwok, R. (2021). Assessment of ICESat-2 sea ice surface classification with sentinel-2 imagery: Implications for freeboard and new estimates of lead and floe geometry. *Earth and Space Science*, *8*(3), e2020EA001491. https://doi.org/10.1029/2020ea001491

Petty, A. A., Holland, P. R., & Feltham, D. L. (2014). Sea ice and the ocean mixed layer over the Antarctic shelf seas. *The Cryosphere*, *8*(2), 761–783. https://doi.org/10.5194/tc-8-761-2014

Petty, A. A., Kwok, R., Bagnardi, M., Ivanoff, A., Kurtz, N., Lee, J., & Hancock, D. (2021). *Atlas/ICESat-2 l3b daily and monthly gridded sea ice freeboard (version 2)*. NSIDC: National Snow and Ice Data Center.

Pfirman, S., Lange, M., Wollenburg, I., & Schlosser, P. (1990). Sea ice characteristics and the role of sediment inclusions in deep-sea deposition: Arctic-Antarctic comparisons. In *Geological history of the polar oceans: Arctic versus Antarctic* (pp. 187–211). Springer. https://doi.org/10.1007/978-94-009-2029-3_11

Rembauville, M., Briggs, N., Ardyna, M., Uitz, J., Catala, P., Penkerc'h, C., et al. (2017). Plankton assemblage estimated with bgc-argo floats in the Southern Ocean: Implications for seasonal successions and particle export. *Journal of Geophysical Research: Oceans*, *122*(10), 8278–8292. https://doi.org/10.1002/2017jc013067

Roemmich, D., Johnson, G. C., Riser, S., Davis, R., Gilson, J., Owens, W. B., et al. (2009). The Argo program: Observing the global ocean with profiling floats. *Oceanography*, *22*(2), 34–43. https://doi.org/10.5670/oceanog.2009.36

Scheick, J., Arendt, A., Heagy, L., & Perez, F. (2019). Introducing icepyx, an open source python library for obtaining and working with ICESat-2 data. *Earth and Space Science*.

Scheick, J., Arendt, A. A., Heagy, L. J., Paolo, F., Perez, F., & Steiker, A. E. (2019). *icepyx: Python tools for obtaining and working with ICESat-2 data*. Retrieved from https://github.com/icesat2py/icepyx

Tagliabue, A., & Arrigo, K. R. (2006). Processes governing the supply of iron to phytoplankton in stratified seas. *Journal of Geophysical Research: Oceans*, *111*(C6). https://doi.org/10.1029/2005jc003363

Vignon, É., Roussel, M.-L., Gorodetskaya, I., Genthon, C., & Berne, A. (2021). Present and future of rainfall in Antarctica. *Geophysical Research Letters*, *48*(8), e2020GL092281. https://doi.org/10.1029/2020gl092281

Wang, S., Bailey, D., Lindsay, K., Moore, J., & Holland, M. (2014). Impact of sea ice on the marine iron cycle and phytoplankton productivity. *Biogeosciences*, *11*(17), 4713–4731. https://doi.org/10.5194/bg-11-4713-2014

Yoshida, K., Seger, A., Kennedy, F., McMinn, A., & Suzuki, K. (2020). Freezing, melting, and light stress on the photophysiology of ice algae: Ex situ incubation of the ice algal diatom *fragilariopsis cylindrus* (bacillariophyceae) using an ice tank. *Journal of Phycology*, *56*(5), 1323–1338. https://doi.org/10.1111/jpy.13036